

Myasthenia Gravis Diagnosis with Surface-enhanced Raman Spectroscopy

Iuliia Riabenko^{1*}, Serhiy Prokhorenko², Elena Klimova³, Konstantin Beloshenko¹.

¹*School of radiophysics, biomedical electronics and computer systems, V. N. Karazin Kharkiv National University, Freedom Square, 4, Kharkiv, 61000, Ukraine.*

²*Faculty of Mathematics and Applied Physics, Rzeszow University of Technology, al. Powstancow Warszawy 8., Rzeszow, 35-959, Poland.*

³*Laboratory of molecular and cellular technologies, State Institution "Institute of General and Emergency Surgery named after V.T. Zaitsev of the National Academy of Medical Sciences of Ukraine", Balakireva, 1, Kharkiv, 61018, Ukraine.*

*jriabenko@karazin.ua

Myasthenia Gravis Diagnosis with Surface-enhanced Raman Spectroscopy

The investigation addresses challenges in diagnosing myasthenia gravis, a condition associated with high mortality rates. Employing the SERS method, blood serum samples were analyzed on quartz glass with implanted gold nanoparticles of about 5 nm. Minuscule dimensions of nanoparticles contribute to the heightened enhancement of Raman signals through interband transitions. The enhanced signals facilitated the detection of peaks observed solely in the blood serum of patients suffering from myasthenia gravis. Peak analysis revealed a spectrum indicating the presence of botulinum toxin-A, the modes of which are coupled with the symmetric nitro stretch and nitro bending modes of the NO₂ group, influencing their positions within the spectrum. Thus, minor changes in the concentrations of compounds acting as markers of diseases can be detected, aiding early diagnosis or express analysis. This approach holds promise for biosensing based on resonance structures to detect pathogens in diverse biosamples.

Keywords: SERS, biosensors, blood serum, myasthenia gravis, botulinum toxin-A.

Introduction

Myasthenia gravis represents the most prevalent neuromuscular junction disorder, posing challenges in diagnosis and contributing to elevated mortality rates [1], yet its understanding remains incomplete [2, 3]. Diagnostic complexities arise primarily during the disease's initial phases, characterized by isolated symptoms or localized weakness [4], progressing proximally to distal muscle weakness [5], with varying specific symptoms. Disease progression may lead to respiratory failure in over 11% of patients, resulting in death in pain [1, 6], while other deaths are often linked to comorbidities potentially triggered by myasthenia gravis [6]. Myasthenia gravis is classified as an autoimmune disorder, characterized by the production of autoantibodies targeting proteins at the neuromuscular junction [7]. However etiological understanding of the

disease remains limited [1], and given its likely higher prevalence than current estimates, efforts are underway to develop diagnostic guidelines based on observable signs [8]. However, existing diagnostic methods, including visual assessments and scales, exhibit varying degrees of inaccuracy. In instances of diplopia, facial ptosis, or muscle weakness, testing for acetylcholine receptor antibodies aids in confirming the diagnosis of ocular or generalized myasthenia gravis, although its clinical sensitivity is only 50 – 70% [9]. While single-fiber electromyography is an accurate method for diagnosing myasthenia gravis in cases of diplopia [10], only 50% of myasthenia gravis patients exhibit ptosis and isolated ocular manifestations as initial symptoms [11], making early diagnosis challenging. The administration of a proserin test is necessary to confirm the diagnosis in later stages or cases of generalized myasthenia gravis [12].

In recent years, there has been a notable increase in the application of surface-enhanced Raman spectroscopy (SERS) as a diagnostic tool [13]. SERS offers numerous advantages, including expediting experiments, enhancing convenience, and facilitating non-destructive testing with exceptional sensitivity [14]. The use of SERS for analyzing blood serum samples to detect various diseases is steadily gaining momentum [15, 16]. Conventional SERS typically yields gains of 10^3 – 10^6 . Nevertheless, the reduction in nanoparticle size and the intensification of oscillations between the substrate and the sample categorize SERS as a nanoscale and single-molecule analytical biochemistry tool [17, 18].

The enhancement factor of the electromagnetic field depends on the gains of both the local field of laser radiation and the plasmon field [19]. Amplification is significantly influenced by the distance between the metal granule and the molecule, as well as by the radius of the nanoparticle [20]. It is important to note that the increase in the cross-section of molecules is enhanced by considering the natural frequency of

oscillations of the free electron in metal nanoparticles, known as the Froehlich frequency, at which resonance is achieved [21]. This resonance takes into account the shape factor of the nanoparticle, which is dependent on the nanoparticle's radius. The optical properties of the composite medium are determined by the permittivity, which is influenced by both the imaginary and real components. These components depend on the refractive and absorption indices, and also take into account the filling factor of the medium [22].

Consequently, to ensure stability and accurate data interpretation in SERS applications, it is essential to consider all parameters that can impact signal amplification. Factors such as the filling factor of the medium, nanoparticle concentration, and nanoparticle size are crucial. Additionally, fixed nanoparticle coordinates are vital for maintaining field localization stability. Hence, in this study focusing on amplifying signals from blood serum samples, substrates were employed instead of synthesized nanoparticles in solution.

Material and methods

The samples were prepared following the protocol outlined in [23], along with the procedure for preparing a substrate with implanted gold nanoparticles [24].

Manufacturing resonant structures

Although various methods exist for fabricating SERS substrates [25, 26], we employed a technique to develop a novel substrate that we deem both cost-effective and convenient. The filling factor of the substrate sublayer with gold optical films was investigated using AFM, revealing a factor of $q = 0.07$ [27]. Quartz substrates were chosen because the Raman shift of quartz crystal lattice falls within the range of 300 –

500 cm^{-1} [28]. The Raman scattering band within the wave number range of 600 to 700 cm^{-1} is attributed to the incident wave scattering through gold nanoparticles, where plasmon oscillations are excited at a frequency of $\omega_p = 9.02\text{ eV}$ [29]. This mechanism facilitates the detection of Raman shifts exceeding 500 cm^{-1} .

Preparation of biological specimens

The study involved 120 patients, including 16 female and 14 male patients with myasthenia gravis, 17 female and 13 male patients with thymoma-associated myasthenia gravis and 30 female and 30 male participants in the control group. The average age of the female population was 49 ± 8.4 years, for the male population it was 46 ± 7.6 years. Blood sampling was carried out from patients undergoing outpatient treatment at the Zaycev V. T. Institute of General and Emergency Surgery of the National Academy of Medical Sciences of Ukraine in accordance with the Helsinki Declaration of the World Medical Association. The studies were approved by the Ethics Committee of Zaycev V. T. Institute of General and Emergency Surgery.

In order to produce the serum, fasting blood was collected from the ulnar vein and placed in a BD - Vacutainer tube with Na-heparin. The sample consisted of 2 tubes of 6 – 8 mL each. The technology for serum production was based on centrifugation using SM-5 MIKROMED (gravity field - 2000 g, exposure - 15 times). Using a Pasteur pipette, the liquid component (the serum) was transferred into a clean polypropylene tube immediately after centrifugation. The serum was further divided into aliquots of 1.5 mL. Before carrying out spectral analysis, it was taken to the laboratory in sterile Eppendorf Tubes 5.0 mL of amber color. Transportation was performed at -20°C while avoiding any drop in temperature or unfreezing. For the control group, samples were also frozen and subsequently studied on the substrate at the same intervals as the

samples from patients suffering from myasthenia, namely 5, 10 and 20 days after blood sampling.

Raman Spectroscopy

After being thawed at 20°C, the drops were applied to the substrate and dried for 12 minutes using a VUP-5M vacuum evaporator with a residual pressure of 1.33 Pa. The measurement range for Raman shift analysis spanned from 150 to 3200 cm⁻¹, with a spectral resolution of 2 cm⁻¹ using the inVia confocal Raman microscope (Renishaw plc, Gloucestershire, UK). The detector employed was a Renishaw CCD camera, boasting dimensions of 1040×256 pixels. The laser source utilized was the I0785SR0090B-IS1 (Innovative Photonic Solutions, New Jersey, USA) operating at a wavelength of 785 nm (mode: normal), with a spectral width of <100 MHz (<0.2 pm, <0.005 cm⁻¹) and an output power of 90 mW. The laser power was set at 1%, and a grid of 1200 lines per mm (633/780) was employed. The exposure time was set at 10 s, utilizing a lens with a magnification factor of 5x. The software utilized for spectrum acquisition was WiRE™ 3.4, followed by processing using WiRE™ 5.6 (Renishaw plc, Gloucestershire, UK).

Results

Blood serum drops from patients with myasthenia gravis, with or without thymoma, are depicted in Fig. 1, captured using the Zeiss™ Primo Star HAL LED microscope (Carl Zeiss Microscopy GmbH, Jena, Germany). The mechanism of organic molecules distribution in drops can be described based on their molar mass. The Gorsky effect [30] of upward diffusion is observed when the drop is drying. Molecules with a higher molar mass are then accumulated at the periphery of the drop. Water and other light components evaporate while drying which shows where to focus the laser beam and

how the microscope system should be set up to successfully detect the spectra.

Additionally, microphotographs of dried drops of blood serum have been added to the supplemental material. The map for Raman spectroscopy measurement provided that delineates the division of blood drops into segments, establishing the measurement methodology is presented in Fig. 2.

The gold nanoparticles implanted into SiO_2 , situated at a depth of 5 nm beneath the flat surface of the fused quartz glass, constitute a high-quality resonance system ($Q \sim 0.8 - 0.9$) with a resonance plasmon frequency of $3.31 \times 10^{15} \text{ s}^{-1}$ [23]. These nanoparticles create a system of coupled oscillators with the serum monolayer [31], resulting in enhanced Raman scattering [32] from a radical group of the organic molecule possessing polarizability.

Raman data have been processed by software WiRE 5.6 that allowed to remove of noise interference and oversaturated spectra. The non-informative part of the spectrum was truncated. Cosmic ray removal was performed across the entire spectrum, with the bandwidth set to 3 – 7 pixels. The autofluorescent background was eliminated using an intelligent spline node set to 11. Then the Savitzky–Golay filter was used for spectra smoothing by a 3rd degree polynomial function. The normalization of the spectrum before further analysis and a comparison of different spectra has been applied. The normalization and subtraction of the substrate spectrum was conducted using identical experimental parameters (exposure time and sample position) as the main measurements.

The supplemental material contains an example of a Raman spectrum obtained from the edge of a blood serum drop taken from patients diagnosed with myasthenia gravis. The spectra shifted for ease of comparison. After completing all processing

stages, the spectrum was analyzed based on its position and peak intensity. The WiRE 5.6 software identified peaks in the active spectrum using the basic threshold settings.

The resulting spectrum of the substrate is presented in the supplemental material and result aligns well with existing data [33]. The average spectra of blood serum (Fig. 3) were obtained by calculating and analyzing processed data using OriginPro 8.0 software (OriginLab, Massachusetts, USA), similar to the method described in [34].

The data presented in the average spectrum (Fig. 3) reveal a high intensity of the fundamental modes of the NO₂ molecule. To quantify the occurrence of other peaks in spectroscopic data collected from all samples, it involved calculating the frequency of specific peak occurrences (Fig. 4) across the samples, using Python Programming Language (PSF, Delaware, USA).

The statistical frequency analysis indicates that these measurements were consistently stable. This observation is evident both in terms of peak presence in the samples and the narrow range of peak detection, which ensured to the stability of the SERS method due to the implantation of nanoparticles.

Discussion

Raman scattering is enhanced due to the two-photon process of interaction between the energy of the polariton field, laser radiation, and vibrational symmetric modes. The enhancement of Raman scattering can be estimated as follows [35]:

$$P_{SERS} = G_{SERS} P_{Raman} = G_{SERS}^{Em} G_{SERS}^{Chem} R_{Raman} = \\ = G_{SERS}^{Em} G_{SERS}^{Chem} N \alpha_R(\omega_R, \omega_L) E(\omega_L), \quad (1)$$

where G_{SERS} - coefficient that takes into account the amplification caused by the substrate, which consists of two electromagnetic coefficient G_{SERS}^{Em} and chemical G_{SERS}^{Chem}

Describing the gain factors we get:

$$P_{\text{SERS}} = \frac{\omega_R^4}{32\pi\varepsilon_0 c^3} \frac{|E_{\text{LOC}}(\omega_L)|^2}{|E(\omega_L)|^2} \frac{|E_{\text{LOC}}(\omega_R)|^2}{|E(\omega_R)|^2} N |\alpha_R(\omega_R, \omega_L) E(\omega_L)|^2 \frac{\sigma_k^{\text{das}}}{\sigma_k^{\text{free}}} \quad (2)$$

The effective cross section of Raman scattering of a molecule deposited on a substrate can be described by the equation [36]:

$$\sigma_\alpha(r, \omega) = \frac{16\pi^2 \omega_{fi}}{c E_0^2} |\langle f | H(r, \omega) | i \rangle|^2 \times \delta[h(\omega - \omega_{fi})] \sim \sigma_\alpha^{(0)} \left| 3 \frac{\varepsilon'(\omega)}{\varepsilon''(\omega)} \right|^2 |h(r)|^2, \quad (3)$$

where $\sigma_\alpha^{(0)}$ - is the cross section of free molecules in the absence of metal, $i \rightarrow f$ is the optical transition from state i to f , $\langle f | H(r, \omega) | i \rangle$ - is the matrix Hamiltonian of the interaction of a molecule with a field, $h(r)$ is the gain of the dipole moment of the adsorbed molecule. Then

$$P_{\text{SERS}} = \frac{\omega_R^4}{12\pi\varepsilon_0 c^3} \frac{|E_{\text{LOC}}(\omega_L)|^2}{|E(\omega_L)|^2} \frac{|E_{\text{LOC}}(\omega_R)|^2}{|E(\omega_R)|^2} N |\alpha_R(\omega_R, \omega_L) E(\omega_L)|^2 \left| 3 \frac{\varepsilon'(\omega)}{\varepsilon''(\omega)} \right|^2 |h(r)|^2. \quad (4)$$

In the case of Au [25] $|\varepsilon'(\omega)|/\varepsilon''(\omega) \approx 10^3$, which is an order of magnitude greater than that of other noble metals. It is this fact that determines the choice of gold as the basis of nanoparticles for enhancing Raman scattering by biomolecules.

If the distance between the molecular group and metal granules falls within the range of 20 – 35 nm [31], we can infer the existence of an additional component of polariton energy during Raman scattering of the molecular group. This suggests the presence of a system of coupled oscillators. On the other hand, it is known that the electric field strength in granules is directed perpendicular to the curvature (Fig. 5 a, b) of the metal surface. Thus, the modes of vibration of molecular groups lying in the plane of the substrate will experience maximum amplification. Such modes are the mode of symmetric stretching of the molecular group (Fig. 5).

Both the presence of a peak and its position are crucial in the study of Raman spectra, as the polarizability tensor of a molecule is contingent upon the solution or medium containing the detected component. Therefore, conducting a comparative analysis of the Raman spectra obtained using the WiRE 5.6 spectral database with those sourced from literature [37] could suggest the presence of Botulinum toxin A spectra in the samples. The obtained spectra feature the NO₂ group, which is part of the molecule, exhibiting a stretching mode of the aromatic ring excited with a shift $\Delta\nu = 19\text{ cm}^{-1}$ and $\Delta\nu = 3\text{ cm}^{-1}$, respectively, due to coupling. This shift is insignificant, owing to the difference in energy utilized to alter the polarizability tensor of the medium constituents. A more substantial field localization is necessitated to augment the polarizability of the aromatic ring.

The literature demonstrates that human monoclonal antibodies effectively neutralize several serotypes of botulinum neurotoxin [38, 39], thereby reproducing the antigen binding model. Meanwhile, nitrogen dioxide is participating in numerous biological reactions [40, 41], including pathological ones and it can be detected taking into account its lifetime [42, 43]. However, it can also be identified in the composition of 3-nitrotyrosine, serving as a crucial Raman reporter molecule, which is produced through the nitration of tyrosine with nitric oxide during apoptosis [44]. Furthermore, in the analyzed averaged spectrum, the peaks at 1620 cm⁻¹ and 1649 cm⁻¹ exhibit less prominence. These peaks have been previously documented in the literature for botulinum toxin detection using the SERS method with labeling, wherein polyclonal animal antibodies were employed to create the label [45]. However, in the context of measuring a signal in humans, this approach yields a lower signal-to-blank ratio.

In view of the above and considering that biochemical investigations of blood parameters [46] and cytokine profiling of immune responses in myasthenia gravis

patients have revealed molecular processes akin to those observed in botulinum toxin poisoning [47 – 50]. The accumulation of botulinum toxin in various organs, including the brain [51], can trigger primary myasthenia gravis symptoms by affecting the innervation of extraocular muscles, resulting in ptosis and paralysis. Our study underscores the need for further research into the potential link between exposure to low concentrations of botulinum toxin and the onset of myasthenia gravis, while emphasizing that the production of antibodies against acetylcholine is not inherently linked to the disease's etiology.

Conclusion

The efficacy of utilizing Raman scattering to identify markers of myasthenia gravis has been validated. By employing implanted nanoparticles into the surface layer of fused quartz, it becomes feasible to capture signals of varying polarization, thereby demonstrating that the local field emanating from metallic gold nanoparticles enhances the Raman scattering of pathological compounds present in the blood serum of myasthenia gravis patients. It has been ascertained that spectra indicative of the presence of botulinum toxin A are discernible in the blood of these patients. The intricate structure of toxins in relation to Raman spectroscopy serves as a critical attribute, as it manifests through multiple bands, consequently heightening the reliability of the outcomes. Nevertheless, it is precisely through analyzing the position of the Raman scattering band from various molecular groups, while considering the oscillation between the medium's components, that assertions about the constituent elements can be made even without the direct "fingerprint" of entire molecules. Therefore, the above analysis of peaks and the results of the search for a known spectrum are worthy of special attention in the future. Conducting additional

spectroscopic studies, in which the infection processes with botulinum toxin A will be simulated, with its controlled residual concentrations on the proposed substrates, would level out the limitations of such analysis from WiRE software. Also, based on the literature data, to determine the membership of the NO₂ group in future studies at different stages of myasthenia, it is essential to control ascorbic and uric acids, protein thiol groups, and the reserves of alpha-tocopherol, bilirubin and ubiquinol-10 [52]. Control of a subpopulation is also possible T cells [53] and a subpopulation of lymphocytes [54] to test the hypothesis of the immune response development mechanism put forward.

In Memoriam:

The authors gratefully acknowledge the significant contributions of Professor V. M. Shulga from the College of Electronic Science and Engineering, Jilin University, China. Professor Shulga was a distinguished expert in physics specializing in electrodynamics and metamaterials, and he played a pivotal role in guiding the theoretical framework and experimental design of this research project. Sadly, Professor Shulga passed away before the completion of this manuscript. We dedicate this article to his memory and recognize his enduring impact on our field.

Acknowledgments:

The authors would like to thank Dr. Eng. Dariusz Żak from the Department of Functional Materials at Rzeszow University of Technology for his valuable assistance in conducting spectral measurements for this research. His expertise and support were instrumental in the successful completion of this study.

Declaration of Interest Statement:

The authors declare that they have no conflicts of interest that could influence the research presented in this manuscript.

References

1. Chen J, Tian DC, Zhang C, Li Z, Zhai Y, Xiu Y, Gu H, Li H, Wang Y, Shi FD. Incidence, mortality, and economic burden of myasthenia gravis in China: A

- nationwide population-based study. *Lancet Reg Health West Pac.* 2020 Nov 27;5:100063. doi: 10.1016/j.lanwpc.2020.100063.
- 2. Brennan J, et al. "Focus on: Myasthenia gravis." *Nursing made Incredibly Easy* 16.2 (2018): 44-49.
 - 3. Bubuioc AM, Kudebayeva A, Turuspeкова S, Lisnic V, Leone MA. The epidemiology of myasthenia gravis. *J Med Life.* 2021 Jan-Mar;14(1):7-16. doi: 10.25122/jml-2020-0145.
 - 4. Sheet, Myasthenia Gravis Fact. "National Institute of Neurological Disorders and Stroke (NINDS)." (2013).
 - 5. Gilhus NE, Verschueren JJ. Myasthenia gravis: subgroup classification and therapeutic strategies. *Lancet Neurol.* 2015 Oct;14(10):1023-36. doi: 10.1016/S1474-4422(15)00145-3.
 - 6. Westerberg E, Punga AR. Mortality rates and causes of death in Swedish Myasthenia Gravis patients. *Neuromuscul Disord.* 2020 Oct;30(10):815-824. doi: 10.1016/j.nmd.2020.08.355. Epub 2020 Aug 12.
 - 7. Lazaridis K, Tzartos SJ. Autoantibody Specificities in Myasthenia Gravis; Implications for Improved Diagnostics and Therapeutics. *Front Immunol.* 2020 Feb 14;11:212. doi: 10.3389/fimmu.2020.00212.
 - 8. Guidon AC, et al. Telemedicine visits in myasthenia gravis: Expert guidance and the Myasthenia Gravis Core Exam (MG-CE). *Muscle & nerve,* 64(3), 270-276 (2021).
 - 9. Peeler CE, De Lott LB, Nagia L, Lemos J, Eggenberger ER, Cornblath WT. Clinical Utility of Acetylcholine Receptor Antibody Testing in Ocular Myasthenia Gravis. *JAMA Neurol.* 2015 Oct;72(10):1170-4. doi: 10.1001/jamaneurol.2015.1444.
 - 10. Sarrigiannis PG, Kennett RP, Read S, Farrugia ME. Single-fiber EMG with a concentric needle electrode: validation in myasthenia gravis. *Muscle Nerve.* 2006 Jan;33(1):61-5. doi: 10.1002/mus.20435.
 - 11. Grob D, Arsura EL, Brunner NG, Namba T. The course of myasthenia gravis and therapies affecting outcome. *Ann N Y Acad Sci.* 1987;505:472-99. doi: 10.1111/j.1749-6632.1987.tb51317.x.
 - 12. Kozyolkina OA, Vizir IV, Sikorskaya MV. "Neurology tests." (2019).
 - 13. Mandal P, Tewari BS. Progress in surface enhanced Raman scattering molecular sensing: A review. *Surfaces and Interfaces,* 28, 101655 (2022).

14. Zhuang J, et al. SERS-based CRISPR/Cas assay on microfluidic paper analytical devices for supersensitive detection of pathogenic bacteria in foods. *Biosensors and Bioelectronics*, 207, 114167 (2022).
15. Gao S, et al. Label-free surface enhanced Raman spectroscopy analysis of blood serum via coffee ring effect for accurate diagnosis of cancers. *Spectrochimica Acta Part A: Molecular and Biomolecular Spectroscopy* 267 (2022): 120605.
16. Kralova K, et al. Comparative study of Raman spectroscopy techniques in blood plasma-based clinical diagnostics: A demonstration on Alzheimer's disease. *Spectrochimica Acta Part A: Molecular and Biomolecular Spectroscopy* 304 (2024): 123392.
17. Kneipp J, Kneipp H, Kneipp K. SERS—a single-molecule and nanoscale tool for bioanalytics. *Chemical Society Reviews*, 37(5), 1052– (2008).
doi:10.1039/b708459p
18. Nie S. Probing Single Molecules and Single Nanoparticles by Surface-Enhanced Raman Scattering. *Science*, 275(5303), 1102–1106 (1997).
doi:10.1126/science.275.5303.1102
19. Cialla-May D, Schmitt M, Popp J. Theoretical principles of Raman spectroscopy. *Physical Sciences Reviews* 4.6 (2019): 20170040.
20. Emel'yanov VI, Koroteev NI. Giant Raman scattering of light by molecules adsorbed on the surface of a metal. *Soviet Physics Uspekhi* 24.10 (1981): 864.
21. Bohren CF, Huffman DR. Absorption and scattering of light by small particles. *John Wiley & Sons*, 2008.
22. Miloslavsky VK, et al. Optical properties of nanostructures. *Functional Materials* 15.3 (2008): 313.
23. Butler HJ, et al. Using Raman spectroscopy to characterize biological materials. *Nat Protoc.* 2016 Apr;11(4):664-87. doi: 10.1038/nprot.2016.036.
24. Zheng Y, et al. Optical properties of colloidal gold nanoparticles implemented into a subsurface layer of fused silica. *Ukrainian journal of physical optics*, (18, № 2), 102-108 (2017).
25. Le Ru EC, Blackie E, Meyer M, Etchegoin PG. Surface enhanced Raman scattering enhancement factors: a comprehensive study. *The Journal of Physical Chemistry C*, 111(37), 13794-13803 (2007).
26. Li JF, et al. Shell-isolated nanoparticle-enhanced Raman spectroscopy. *nature*, 464(7287), 392-395 (2010).

27. Riabenko I, et al. Permittivity Model Selection Based on Size and Quantum-Size Effects in Gold Films. *East European Journal of Physics*, no. 3, Sept. 2023, pp. 406-12, doi:10.26565/2312-4334-2023-3-44.
28. Tuschel D. Selecting an excitation wavelength for Raman spectroscopy. *Spectroscopy*, 31(3), 14-23 (2016).
29. Ordal MA, et al. Optical properties of fourteen metals in the infrared and far infrared: Al, Co, Cu, Au, Fe, Pb, Mo, Ni, Pd, Pt, Ag, Ti, V, and W. *Applied optics*, 24(24), 4493-4499 (1985).
30. Völkl J. The gorsky effect. *Berichte der Bunsengesellschaft für physikalische Chemie*, 76(8), 797-805 (1972).
31. Wan J, et al. Resonance light absorption of granular aluminium and silver films placed on a rough sublayer of multilayered ZnS. *Ukrainian journal of physical optics*, (20, № 1), 10-15 (2019).
32. Chang R. Surface enhanced Raman scattering. Springer Science & Business Media (2013).
33. Tuschel D. Why are the Raman spectra of crystalline and amorphous solids different?. *Spectroscopy* 32.3 (2017): 26-33.
34. Riabenko I, et al. Physiotherapy in the treatment of the metabolic syndrome associated with the right-sided scoliosis. *Physical rehabilitation and recreational health technologies* 8.3 (2023): 136-143.
35. Pilot R, et al. A Review on Surface-Enhanced Raman Scattering. *Biosensors (Basel)*. 2019 Apr 17;9(2):57. doi: 10.3390/bios9020057.
36. Koningstein JA. Introduction to the Theory of the Raman Effect. Springer Science & Business Media (2012).
37. Lim CY, Granger JH, Porter MD. SERS detection of Clostridium botulinum neurotoxin serotypes A and B in buffer and serum: Towards the development of a biodefense test platform. *Analytica Chimica Acta: X* 1 (2019): 100002.
38. (a) Fan Y, et al. Monoclonal antibodies targeting the alpha-exosite of botulinum neurotoxin serotype/A inhibit catalytic activity. *PLoS One* 10.8 (2015): e0135306. (b) Monoclonal antibodies that inhibit the proteolytic activity of botulinum neurotoxin serotype/B. *Toxins* 7.9 (2015): 3405-3423.
39. Garcia-Rodriguez C, et al. A three monoclonal antibody combination potently neutralizes multiple botulinum neurotoxin serotype E subtypes. *Toxins* 10.3 (2018): 105.

40. Sharma VK, Manoli K, Ma X. Reactivity of nitrogen species with inorganic and organic compounds in water. *Chemosphere* 302 (2022): 134911.
41. Yoshida K, Kasama K. Biotransformation of nitric oxide. *Environmental Health Perspectives* 73 (1987): 201-205.
42. Ford E, Hughes MN, Wardman P. Kinetics of the reactions of nitrogen dioxide with glutathione, cysteine, and uric acid at physiological pH. *Free Radical Biology and Medicine* 32.12 (2002): 1314-1323.
43. (a) Goldstein S, Merenyi G. The chemistry of peroxynitrite: implications for biological activity. *Methods in enzymology* 436 (2008): 49-61. (b) The reaction of NO· with O₂·– and HO₂·–: A pulse radiolysis study." *Free Radical Biology and Medicine* 19.4 (1995): 505-510.
44. Pacher P, Beckman JS, Liaudet L. Nitric oxide and peroxynitrite in health and disease. *Physiological reviews* 87.1 (2007): 315-424.
45. Kim K, et al. SERS-based immunoassays for the detection of botulinum toxins A and B using magnetic beads. *Sensors* 19.19 (2019): 4081.
46. Gounden V, Vashisht R, Jialal I. Hypoalbuminemia. StatPearls. Treasure Island (FL): StatPearls Publishing; 2020. Available: <http://www.ncbi.nlm.nih.gov/books/NBK526080/>.
47. Maurer M, et al. IL-6 and Akt are involved in muscular pathogenesis in myasthenia gravis. *Acta Neuropathol Commun.* 2015 Jan 15;3:1. doi: 10.1186/s40478-014-0179-6.
48. Aricha R, et al. Blocking of IL-6 suppresses experimental autoimmune myasthenia gravis. *J Autoimmun.* 2011 Mar;36(2):135-41. doi: 10.1016/j.jaut.2010.12.001.
49. Punga AR, Liik M. Botulinum toxin injections associated with suspected myasthenia gravis: An underappreciated cause of MG-like clinical presentation. *Clin Neurophysiol Pract.* 2020 Feb 7;5:46-49. doi: 10.1016/j.cnp.2020.01.002.
50. Seo MS, et al. Comparison study of the response with botulinum toxin muscle injection in the ICR mice from three different sources. *Lab Anim Res.* 2019 Jul 26;35:11. doi: 10.1186/s42826-019-0010-4.
51. Hart LG, Dixon RL, Long JP, Mackay B. Studies using Clostridium botulinum toxin—Type A. *Toxicology and Applied Pharmacology*, 7(1), 84-89 (1965).
52. Halliwell B, et al. Interaction of nitrogen dioxide with human plasma Antioxidant depletion and oxidative damage. *FEBS letters* 313.1 (1992): 62-66.

53. Rutowski J, et al. The effects of occupational exposure to nitrogen dioxide (NO₂) on the immunological parameters in workers. *Medycyna Pracy* 49.4 (1998): 341-351.
54. Backé E, et al. Immunological biomarkers in salt miners exposed to salt dust, diesel exhaust and nitrogen oxides. *International archives of occupational and environmental health* 77 (2004): 319-327.

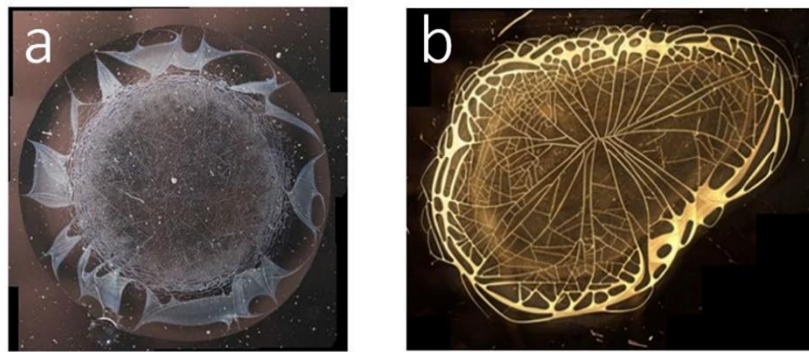


Figure 1. Micrographs of blood serum drops: a) patient with thymoma-associated myasthenia gravis; b) patient with myasthenia gravis.

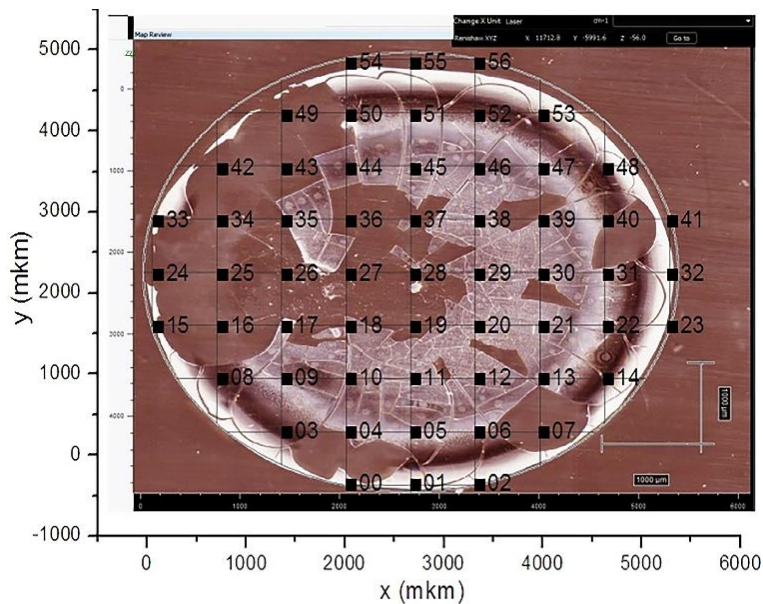


Figure 2. Segmenting blood serum drop samples to acquire spectra from the edges of the drops.

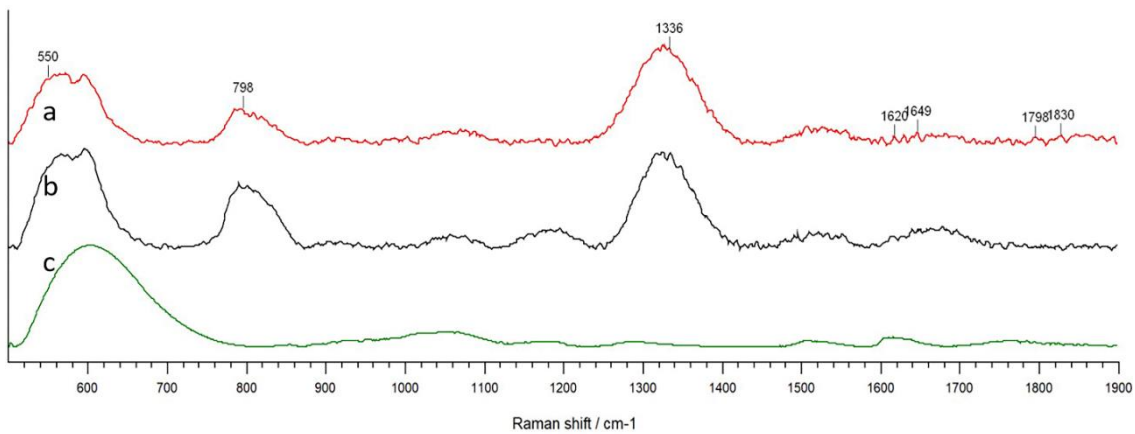


Figure 3. Average Raman spectra in blood serum were observed in: a) patients with myasthenia gravis; b) those with thymoma-associated myasthenia gravis; and c) healthy research participants.

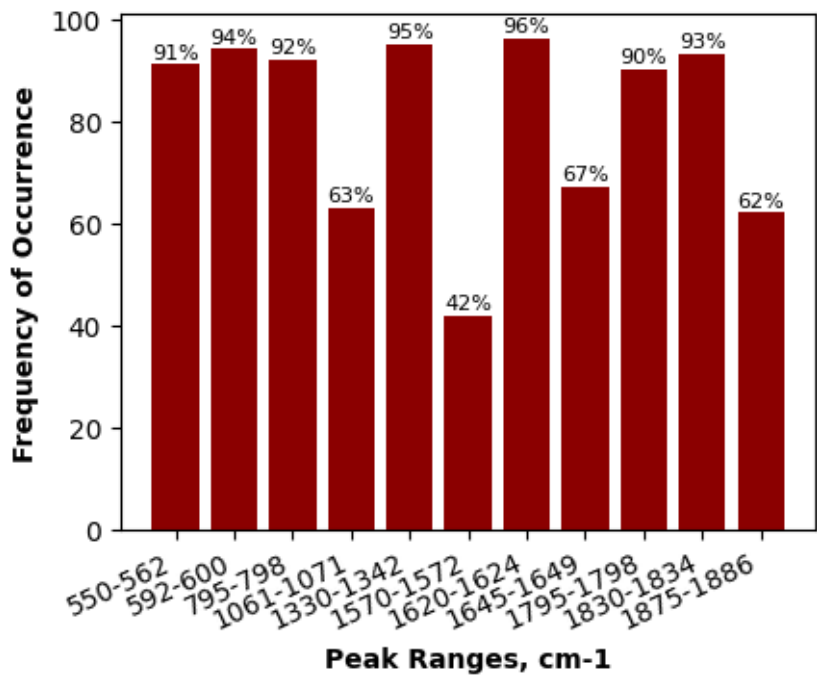


Figure 4. Frequency analysis of specific peak occurrences.

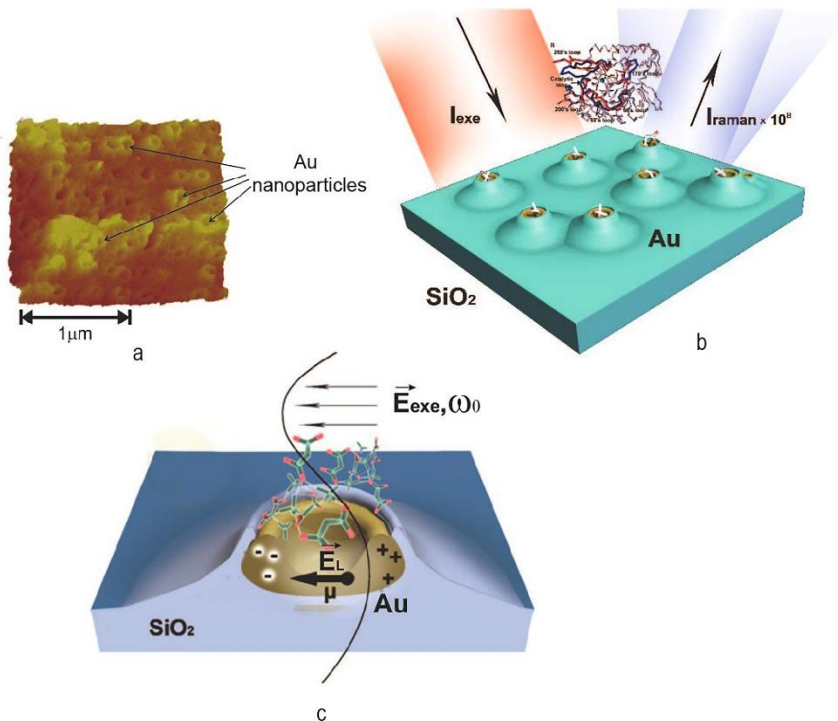


Figure 5. Enhancement of Raman scattering facilitated by implanted nanoparticles: a) AFM image of Au nanoparticles implanted in SiO₂; b) scheme illustrating combined amplification by metal nanoparticles and their interaction with sample components; c) molecular groups of molecules within the vicinity of metal granules.

Supplemental material

Myasthenia Gravis Diagnosis with Surface-enhanced Raman Spectroscopy

Iuliia Riabenko^{1*}, Serhiy Prokhorenko², Elena Klimova³, Konstantin Beloshenko¹.

¹*School of radiophysics, biomedical electronics and computer systems, V. N. Karazin Kharkiv National University, Freedom Square, 4, Kharkiv, 61000, Ukraine.*

²*Faculty of Mathematics and Applied Physics, Rzeszow University of Technology, al. Powstancow Warszawy 8., Rzeszow, 35-959, Poland.*

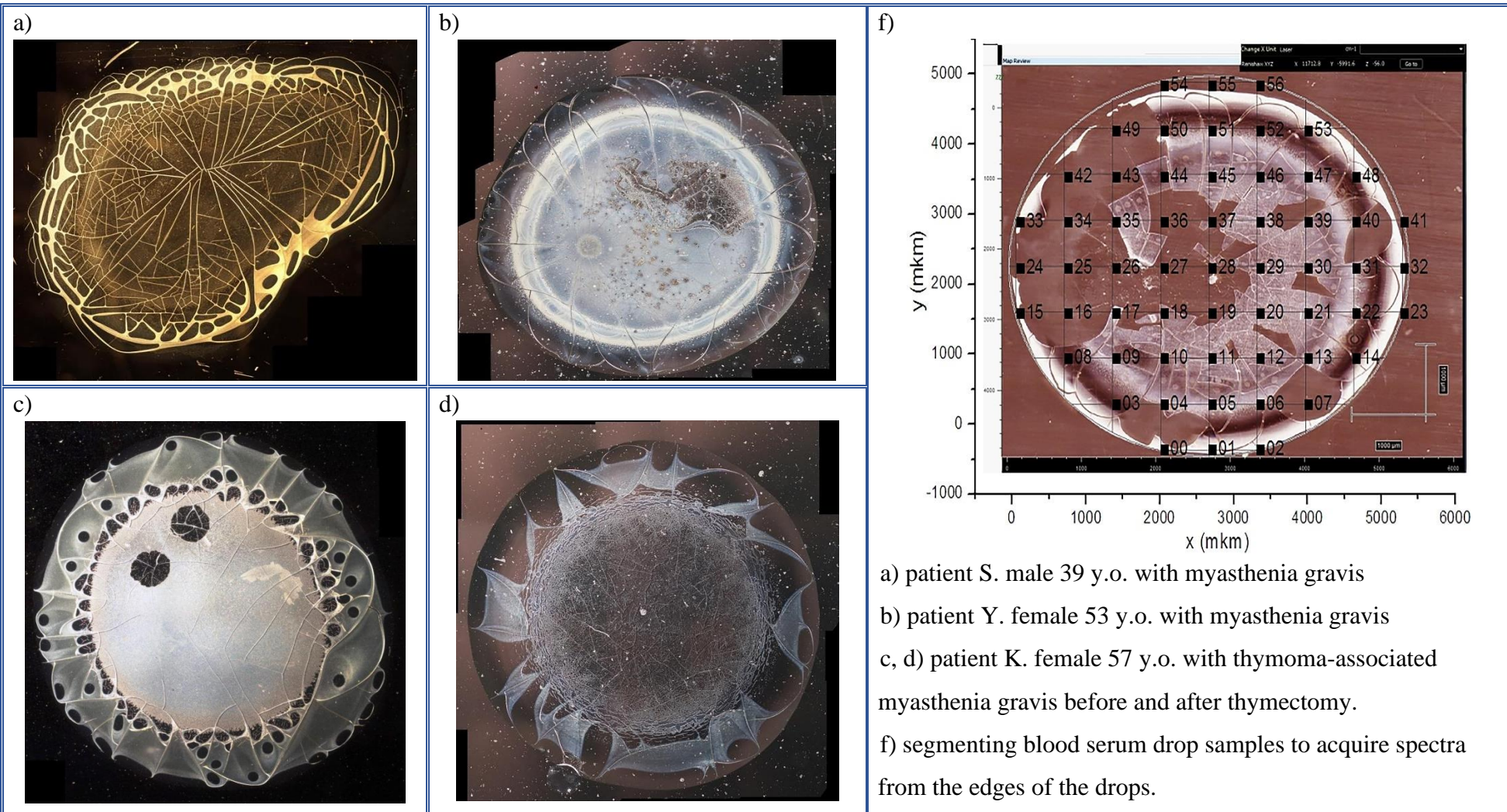
³*Laboratory of molecular and cellular technologies, State Institution "Institute of General and Emergency Surgery named after V.T. Zaitsev of the National Academy of Medical Sciences of Ukraine", Balakireva, 1, Kharkiv, 61018, Ukraine.*

*jriabenko@karazin.ua

Table of Contents

(1) <i>Table S1: Micrographs of blood serum drops and the segmenting blood serum drop samples to establishing the measurement methodology.</i>	<i>SM-2</i>
(2) <i>Figure S1: Peak analysis of Raman spectrum of a fused quartz substrate with gold implantation.</i>	<i>SM-3</i>
(3) <i>Figure S2: Average Raman spectra in blood serum.....</i>	<i>SM-3</i>
(4) <i>Figure S3: Raman spectrum obtained from the edge of a blood serum drop taken from patients diagnosed with myasthenia gravis.....</i>	<i>SM-4</i>
(5) <i>Figure S4: Frequency analysis of specific peak occurrences in the spectra</i>	<i>SM-4</i>
(6) <i>Figure S5: Enhancement of Raman scattering facilitated by implanted nanoparticles</i>	<i>SM-5</i>

Table S1 Micrographs of blood serum drops and the segmenting blood serum drop samples to establishing the measurement methodology.



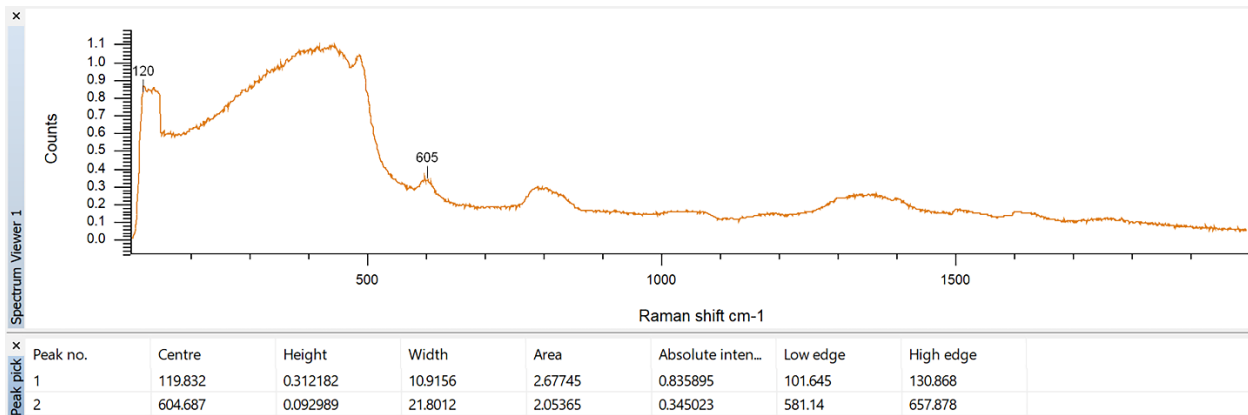


Figure S1. Peak analysis of Raman spectrum of a fused quartz substrate with gold implantation. The resultant spectrum of the substrate exhibits two primary peaks corresponding to metal (120 cm^{-1}) and quartz (605 cm^{-1}). The result aligns well with existing data [35], however, in the case of the metal, the scattering band at the FWHM level is truncated, resembling the shape of a truncated trapezoid.

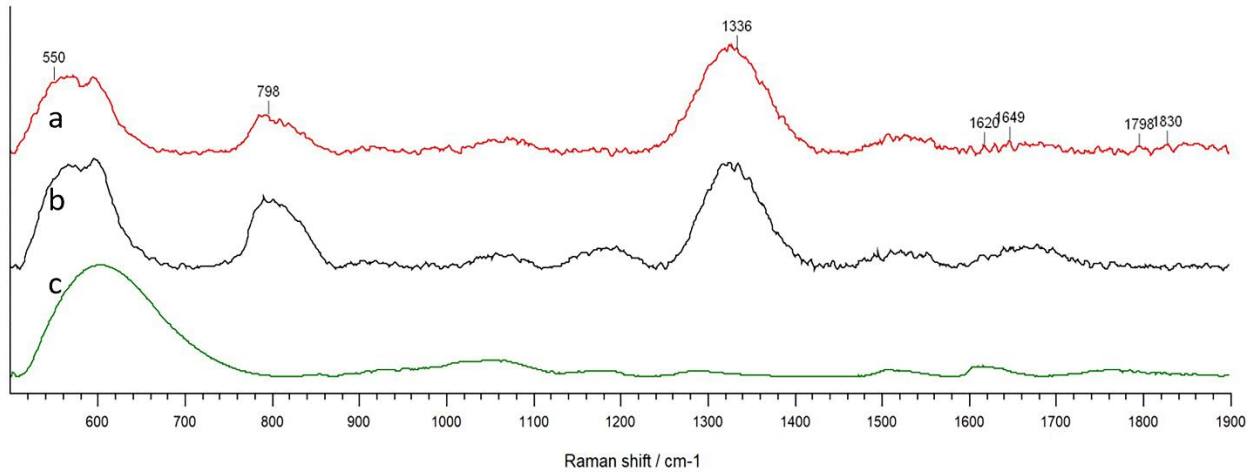


Figure S2. Average Raman spectra in blood serum were observed in:

- a) patients with myasthenia gravis;
- b) those with thymoma-associated myasthenia gravis; and
- c) healthy research participants.

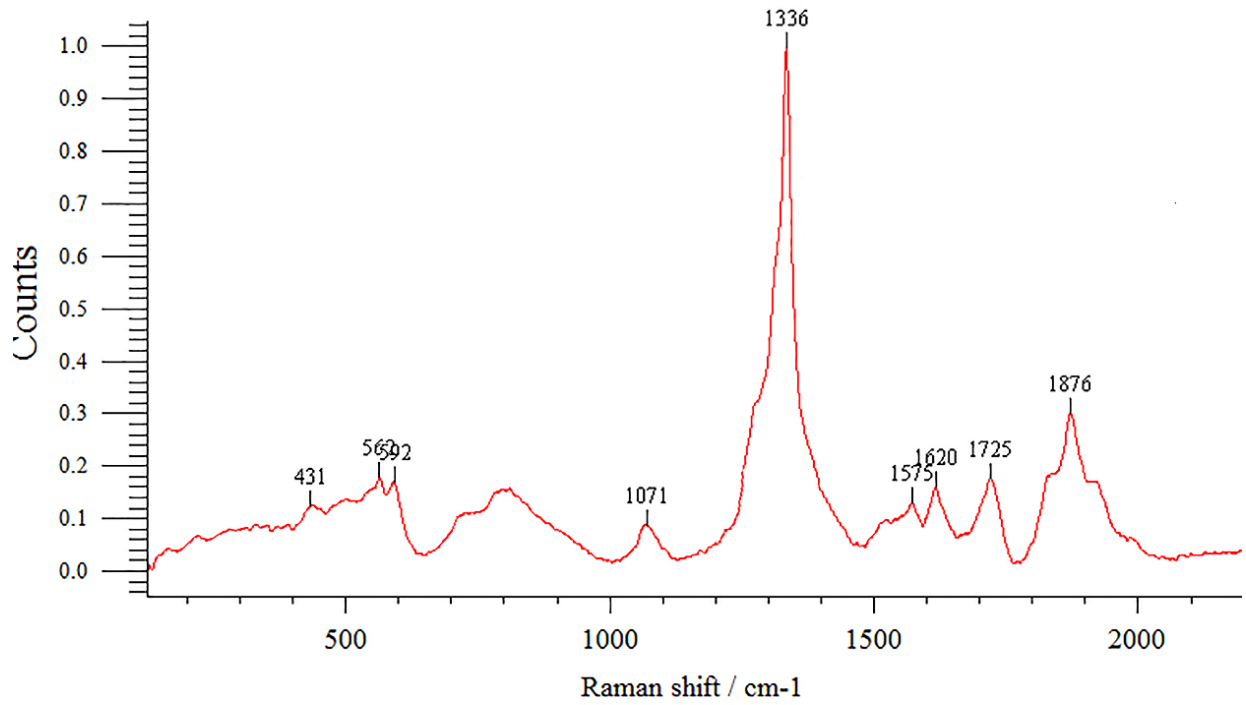


Figure S3. Raman spectrum obtained from the edge of a blood serum drop taken from patients diagnosed with myasthenia gravis.

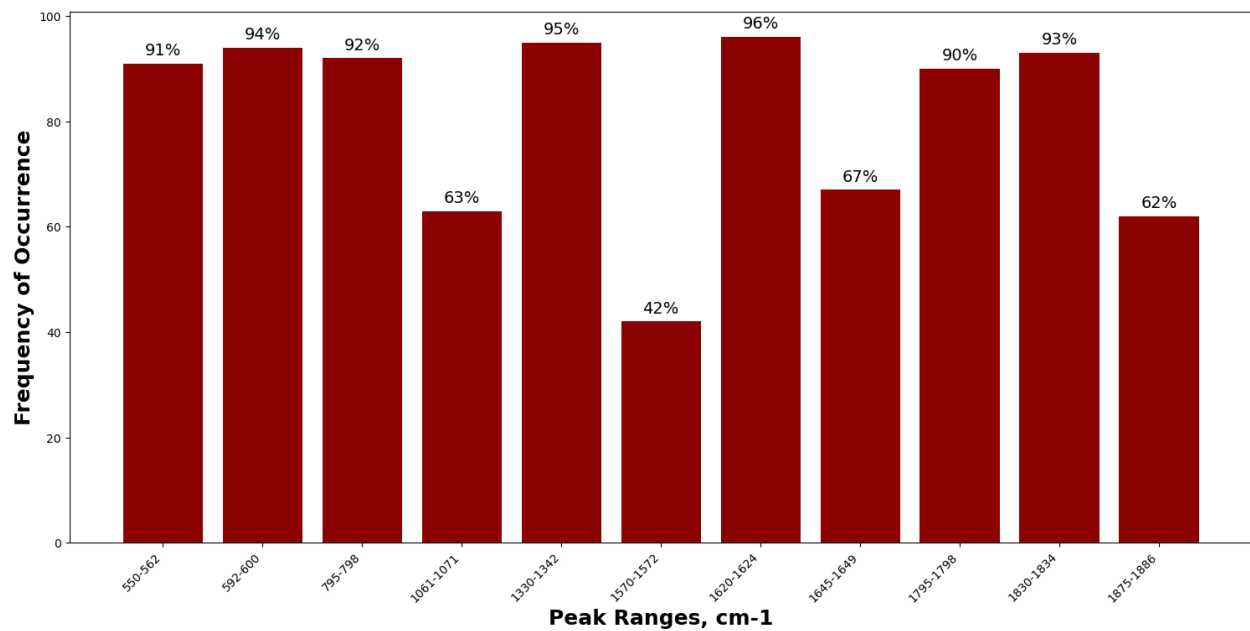


Figure S4. Frequency analysis of specific peak occurrences in the spectra of the edges of a drops of blood serum from all study patients with myasthenia gravis and thymoma-associated myasthenia gravis.

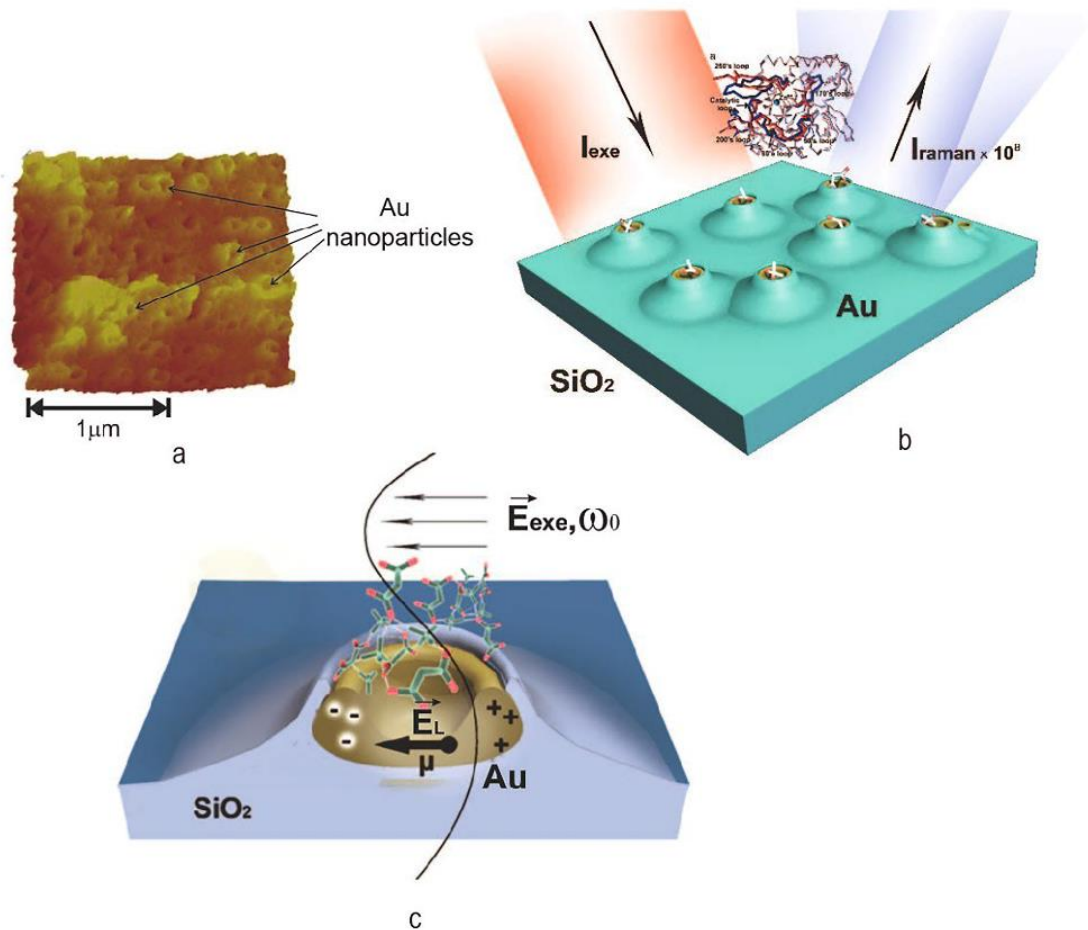


Figure S5. Enhancement of Raman scattering facilitated by implanted nanoparticles:

- a) AFM image of Au nanoparticles implanted in SiO₂;
- b) scheme illustrating combined amplification by metal nanoparticles and their interaction with sample components;
- c) molecular groups of molecules within the vicinity of metal granules.